SENSITIVITY ANALYSIS OF THE ELECTRIC SAIL DEPLOYMENT DYNAMICS PARAMETERS

JoAnna Fulton and Hanspeter Schaub

5th International Conference On Tethers In Space

Sensitivity Analysis of the Electric Sail Deployment Dynamics Parameters

JoAnna Fulton[*] and Hanspeter Schaub [†]

University of Colorado at Boulder, Boulder, CO, 80309

The deployment dynamics of a spin stabilized electric sail (E-sail) with a hub-mounted control actuator are investigated. Both radial and tangential deployment mechanisms are considered to take the electric sail from a post-launch stowed configuration to a fully deployed configuration. The tangential configuration assumes the multi-kilometer tethers are wound up on the exterior of the spacecraft hub, similar to yo-yo despinner configurations. The deployment speed is controlled through the hub rate. The radial deployment configuration assumes each tether is on its own spool. Here both the hub and spool rate are control variables. The sensitivity of the deployment behavior to E-sail length, maximum rate and tension parameters is investigated. A constant hub rate deployment is compared to a time varying hub rate that maintains a constant tether tension condition. The deployment time can be reduced by a factor of 2 or more by using a tension controlled deployment configuration.

I.   Introduction

The E-sail is a novel propellantless in-space propulsion concept with great potential for fast interplanetary and near interstellar missions, invented and proposed by Pekka Janhunen[1] at the Finnish Meteorological Institute. In this concept, a system of radially configured, thin, charged tethers generate an electric field that interacts with solar wind protons to harvest acceleration for spacecraft propulsion, demonstrated in Figure 1. This provides infinite specific impulse and eliminates the need for traditional chemical propellants.[2] Only an electron gun is required to maintain a positive electrostatic charge on the tethers. The positive solar wind ions deflect of the results E-sail tether force field, causing a net force onto the spacecraft. This solar wind propulsion concept is advantageous in comparison to the solar radiation pressure (SRP) based solar sail due to the effective area of the electrostatic forces and improved solar radius dependence.[3] A single charged wire, microns thick, will create a meters-wide effective area, expanding the area of influence of a minimal structure. In comparison, SRP is directly dependent on the physical area of the solar sail, providing many challenges in manufacturing, packaging, and deploying large membranes.[4] The solar radius dependence of the E-sail has been shown to decay the acceleration at $1/r^{7/6}$, slower than that of the solar sail at $1/r^2$. This is encouraging for long distance missions to the outer planets and beyond. However, the E-sail is not operable within a planet's magnetosphere, where the solar wind protons are deflected, whereas a solar sail still accelerates on the photons in this region.

Multiple missions have been designed using the E-sail as the primary propulsion system with encouraging results. A fast entry probe mission to Uranus could be achieved in less than 6 years,[6] the interstellar medium reached in as little as 10 years,[7] and a near Earth asteroid rendezvous could be completed within a year.[8] Additionally, missions to the inner planets, such as Venus and Mars, could also be achieved in less than 1 and 2 years, respectively.[9] This provides adequate motivation to pursue further development of the E-sail system. The electrostatic propulsion theory enabling these missions has been studied. However, the coupled dynamics of the spacecraft and charged tether system is not well understood. Typically, the E-sail systems considered are composed of 20-100 tethers, up to 20 km in length,

---

*Graduate Research Assistant, Aerospace Engineering Sciences, University of Colorado at Boulder, 431 UCB, Colorado Center for Astrodynamics Research, Boulder, CO 80309-0431

†Alfred T. and Betty E. Look Professor of Engineering, Aerospace Engineering Sciences, University of Colorado at Boulder, 431 UCB, Colorado Center for Astrodynamics Research, Boulder, CO 80309-0431
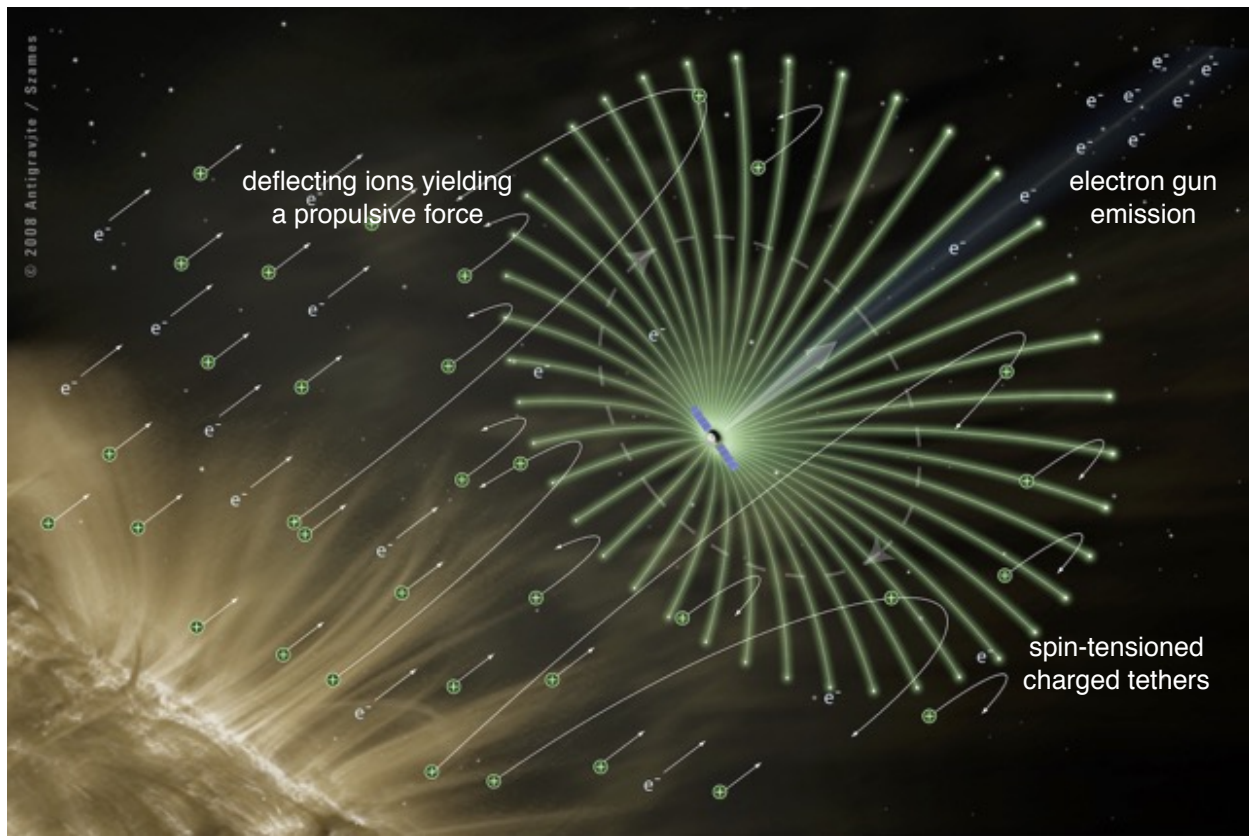
Figure 1: The electrostatic sail is charged by a spin axis-pointed electron beam and deflects solar wind protons to generate thrust. Artist concept image by A. Szames.[5]

with payload masses of 100-2000 kg. These tethers are constructed using multiple micron-thick conductive tethers with auxiliary loops, known as a Hoytether,[10] to provide redundancy and protect against micrometeors. Construction of such tethers at the desired length has been investigated with encouraging results.[11] One such tether, 10 meters in length, was flown on the EstCube-1[12] but was not deployed.[13] Despite this, evidence supporting the feasibility of the E-sail is continuing to develop, and steps will now be taken towards understanding the deployment requirements for such a structure.

During flight, the tethers are spin-stabilized to maintain tensioned, radial, straight line configurations. Therefore, the deployment scheme must settle with the spacecraft and each tether component rotating at equal rates. However, a mass spinning out from a central body will dramatically change the body rates as momentum is exchanged from the body to the deploying mass. For example, a spacecraft-tether system modeled with a spherical pendulum (such as the yo-yo despinner mechanism used on the Dawn mission) will asymptotically approach the negative initial rate if left in free spin. Therefore, energy and momentum must be continually input to the system as the tethers are deploying to prevent large deviations in spin rates. A primary challenge for the E-sail deployment is determining a low-risk scheme to accomplish this, presenting a non-trivial task.

A proposed scheme for the E-sail mounts the tethers at a radial orientation,[14] where each tether is housed with an individual hub and motor subsystem to conduct the tether unspooling. An auxiliary tether would line the periphery of the sail, and thruster units would interface between the tether end points and auxiliary tether to control position and momentum. These components significantly increase the mass budget of the E-sail and introduce a highly complex dynamics problem. In this paper, an auxiliary tether is not included such that only a stand alone end mass is accounted for. Additionally, novel deployment schemes are proposed, where the hub rate is controlled using hub-mounted devices such as electric thrusters. A hub mounted strategy will be much simpler than coordinating and commanding individual tether-mounted devices to actuate deployment. Furthermore, applying torque through the hub can be done using commercially available products, whereas tether end point thruster units are currently under development.

Two deployment schemes that use a hub-mounted energy source are considered. The first is a tangentially aligned

deployment, where all tethers are mounted on a central hub oriented with the spacecraft hub spin axis, taking advantage of the rotational dynamics to deploy the tethers simultaneously. The second deployment scheme uses a radially oriented deployment configuration. Such a configuration has each tether housed on a separate spool and motor device. This paper compares the dynamic deployment behavior of these two methods. The coupled rotational dynamics of the spacecraft hub and E-sail system is modeled during the deployment phase and the control of these dynamics is investigated. The deployment is assumed to occur in a single plane, reducing the problem to rotational degrees of freedoms about the deployment normal axis and ignoring out of plane dynamics. It is also assumed that the spacecraft has reached deep space conditions before initiating deployment, the sail is not charged during deployment, and the tethers do not stick or adhere as they deploy. Of interest is the nominal performance for each deployment type, as well as the sensitivity of this performance with respect to the hub speed and spool reel rate. Numerical simulations demonstrate the expected performance.

II.   Dynamics Modeling

A.   Spacecraft and E-Sail Mass Model

The mass budget of the E-sail and spacecraft system is selected such that the characteristic acceleration of the E-sail at 1 Au from the Sun is between $a_\oplus = 0.1 - 1$ mm s^{-2}. At $a_\oplus = 1$ mm s^{-2}, significantly faster missions to the outer planets and beyond are feasible.[6] The characteristic acceleration is given by:[15]

$$a_\oplus = \frac{fNL}{m} \tag{1}$$

where N is the number of tethers, L is the length of the tethers, m is the total mass of the spacecraft, and f is the thrust per unit tether length at 1 AU from the Sun. Using the physical reference data for the E-sail,[15] this is known to be $f = 579.84$ nN m^{-1} for an E-sail operating at 25 kV nominal tether voltage. The total system mass is set to $m = 500$ kg, a smaller but feasible mass for an interplanetary science mission, to facilitate greater focus on the other free parameters of the system. It is assumed that the maximum number of tethers is 100 and the maximum length of a tether is restricted to 20 km.[15] However, this only slightly restricts the range of E-sail sizes that will yield the desired characteristic acceleration in Eq. (1). For a scenario where there is minimal end mass, no remote devices, and minimal number of tethers with maximum length, the tethers themselves are the largest contribution to the spacecraft system momentum. Therefore, accurate modeling of the E-sail deployment requires that the tether inertia is not treated as negligible and is modeled as a slender rod with total mass equal to the tether mass. This model assumes the tether remains straight, but future models will include discrete points of freedom to increase the fidelity of the flexible body dynamics model. The tether mass is described as a function of the deployment length, where the mass per unit length per tether is assumed to be $\lambda = 1.155 \times 10^{-5}$ kg/m.[15] Where ρ is the mass per unit length for N number of tethers, $\rho = N\lambda$ for a given sail size. The mass of all deploying tethers is then described as:

$$m_T = \rho l = \rho R \phi \tag{2}$$

where l is the deployed length, which can be described in terms of the unwrap angle ϕ and the spacecraft hub radius R for a tangential deployment. The derived tether inertia for each case is included in later sections. The spacecraft is modeled with the additional mass of the stowed portion of the tethers placed along the circumference of the spacecraft. Combining the time varying stowed tether contribution of the inertia to the spacecraft, the inertia of the hub is expressed in the tether fixed $\mathcal{S}$ frame, where only the third axis term will be of a contributor to the planar deployment. This third axis term expressed in the tether frame is the same for all deployment models, where m_H is the hub mass.

$$I_{s_{33}} = \frac{1}{2}m_H R^2 + R^2(m_{T,0} - m_T) \tag{3}$$

B.   Equations of Motion via Lagrange's Equation

The equations of motion for each case are efficiently determined using the Lagrange energy based approach. The kinetic energy of the system is

$$T = T_H + \sum_{i=1}^{N} T_{T,i} + \sum_{i=1}^{N} T_{E,i} = T_H + T_T + T_E \tag{4}$$

where subscript H refers to the spacecraft hub, T refers to the tethers, E refers to the tether end mass, and i indicates an individual tether. Assuming that all N tethers are deployed symmetrically at equal rates and have identical

construction, these summation terms can be reduced to a single lumped term, where the energy contribution of the tether system is equivalent to a single tether of equivalent mass. Similarly, the energy contribution of the end masses is condensed. The kinetic energy of each component is then written as follows:

$$T_H = \frac{1}{2}\boldsymbol{\omega}_{\mathcal{B}/\mathcal{N}}^{\mathsf{T}}[I_s]\boldsymbol{\omega}_{\mathcal{B}/\mathcal{N}} \tag{5a}$$

$$T_T = \frac{1}{2}\boldsymbol{\omega}_{\mathcal{S}/\mathcal{N}}^{\mathsf{T}}[I_T]\boldsymbol{\omega}_{\mathcal{S}/\mathcal{N}} + \frac{1}{2}m_T\dot{\boldsymbol{R}}_{T,C} \cdot \dot{\boldsymbol{R}}_{T,C} \tag{5b}$$

$$T_E = \frac{1}{2}m_E\dot{\boldsymbol{R}}_E \cdot \dot{\boldsymbol{R}}_E \tag{5c}$$

Where the expressions of the inertias, velocities, and rotation rates are defined uniquely for the two cases in subsequent sections. The equations of motion are then derived using Lagrange's Equation. Where there are no potential energy sources, this is simplified to

$$\frac{\mathrm{d}}{\mathrm{d}t}\left(\frac{\partial T}{\partial \dot{q}_j}\right) - \left(\frac{\partial T}{\partial q_j}\right) = Q_{\mathrm{nc}_j} \tag{6}$$

where the non-conservative force is the torque applied on the spacecraft hub. The contribution of this torque to each general coordinate equation is determined as follows.

$$Q_{\mathrm{nc}_j} = \boldsymbol{u}_s \cdot \frac{\partial \boldsymbol{\omega}_{\mathcal{B}/\mathcal{N}}}{\partial \dot{q}_j} \tag{7}$$

III.   Tangential Deployment Method and Parameter Analysis

In this concept, the tethers are deployed tangentially using a free deployment, where the acceleration of the end mass advances the tether, much like with a yo-yo despinner. The phases of this deployment are illustrated in Figure 2. Each of the tethers are wrapped about a central hub and are unreeled from the hub simultaneously. This method takes advantage of the spin stabilized system dynamics to actuate the deployment and relies only on the spacecraft spin rate. Therefore, control of the spacecraft spin rate will couple with the deployment rate, creating a more complex dynamical system but providing a free deployment scheme. Additionally, transitioning the fully deployed tangential tethers to a radial configuration must also be modeled. Therefore, the deployment is operated in two phases, an unwrap phase that releases the tether length, and a hinging phase that transitions the tethers from the tangential to radial configurations.
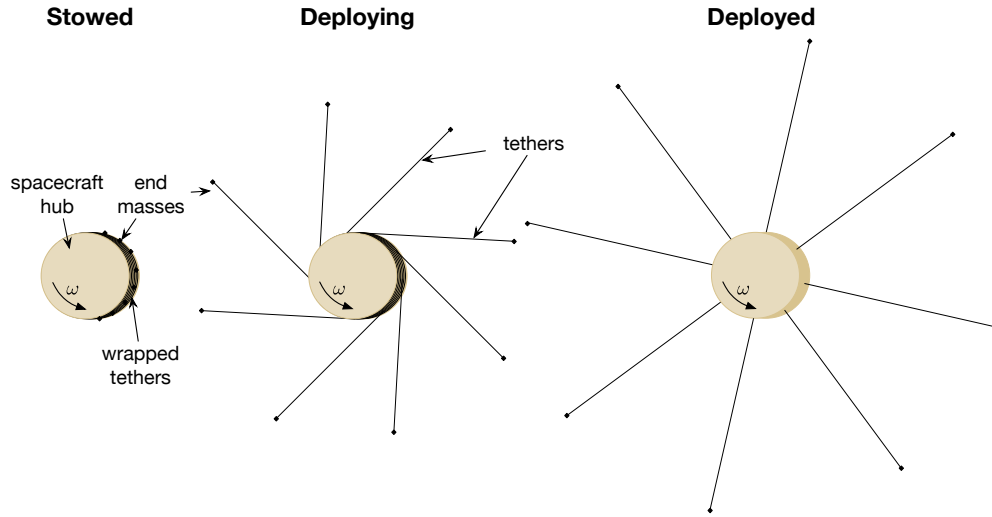

Figure 2: Diagram showing various stages of the tangential deployment scheme

A.   Equations of Motion for Tangential Deployment

A dynamical model of the deployment is developed based on a spacecraft hub based control scheme. This model is primarily concerned with the momentum balance between the spacecraft hub, tethers, and tether end masses, and therefore makes several simplifying assumptions. The tethers and tether end masses are assumed to behave in a symmetrical fashion, and therefore are described using one set of state parameters. The tether is treated as a time varying,

straight slender rod and tether flexibility is not considered in this first order analysis. Such flexible considerations can be addressed in future models by using an N degree of freedom lumped mass model. The parameters of this deployment method are defined in Fig. 3.
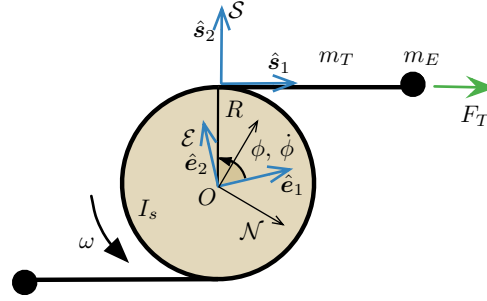

Figure 3: Tangential deployment dynamics parameters

Here ϕ is the deployment unwrap angle, measured from the tether tangent point's original position and ω is the spacecraft rate. Where the rotation rates with respect to the inertial frame are defined as

$$\boldsymbol{\omega}_{\mathcal{B}/\mathcal{N}} = \omega \hat{\boldsymbol{s}}_3 \tag{8}$$

$$\boldsymbol{\omega}_{\mathcal{S}/\mathcal{N}} = (\omega + \dot{\phi})\hat{\boldsymbol{s}}_3 \tag{9}$$

The velocity vectors are determined as

$$\dot{\boldsymbol{R}}_E = -R\omega \hat{\boldsymbol{s}}_1 + R\phi(\omega + \dot{\phi})\hat{\boldsymbol{s}}_2 \tag{10}$$

$$\dot{\boldsymbol{R}}_{T,C} = -\frac{1}{2}R(2\omega + \dot{\phi})\hat{\boldsymbol{s}}_1 + \frac{1}{2}R\phi(\omega + \dot{\phi})\hat{\boldsymbol{s}}_2 \tag{11}$$

Treating the inertia of the tether as a slender rod, and applying the parallel axis theorem, the inertia of the tethers with respect to an origin located at the spacecraft center of mass is shown in Eq. (12), expressed in the tether fixed $\mathcal{S}$ frame.

$$[I_T] = \begin{bmatrix} R^3\rho\phi & -\frac{1}{2}R^3\rho\phi^2 & 0 \\ -\frac{1}{2}R^3\rho\phi^2 & \frac{1}{3}R^3\rho\phi^3 & 0 \\ 0 & 0 & \frac{1}{12}R^3\rho\phi^3 + R\rho\phi(R^2 + \frac{1}{4}R^2\phi^2) \end{bmatrix} \tag{12}$$

These expressions are used to define the kinetic energy expressions of Eq. (5c). Then, the equations of motion are derived using Lagrange's Equation to be as follows. The spacecraft rate, ω, the tether unwrap angle, ϕ, and the unwrap rate, $\dot{\phi}$, are the state coordinates of this system.

$$\frac{1}{24}R^2(-3(4R\rho + 8m_E\phi + 7R\rho\phi^2)\omega^2 + 3(5R\rho + 8m_E\phi + 7R\rho\phi^2)\dot{\phi}) +$$
$$\frac{1}{12}R^2\phi(18R\rho + 12m_E\phi + 7R\rho\phi^2)\dot{\omega} + \frac{1}{12}R^2\phi(15R\rho + 12m_E\phi + 7R\rho\phi^2)\ddot{\phi} = 0 \tag{13}$$

$$\frac{1}{12}R^2(3(4R\rho + 8m_E\phi + 7R\rho\phi^2)\omega\dot{\phi} + 3(6R\rho + 8m_E\phi + 7R\rho\phi^2)\dot{\phi}^2) +$$
$$\frac{1}{12}R^2(6(2m_E + m_H + 2m_{T,0}) + 12R\rho\phi + 12m_E\phi^2 + 7R\rho\phi^3)\dot{\omega} +$$
$$\frac{1}{12}R^2\phi(18R\rho + 12m_E\phi + 7R\rho\phi^2)\ddot{\phi} = u_s \tag{14}$$

These are only applicable to the point where the tethers are fully unwrapped. Following this point, the tethers must transition to a radial orientation with respect to the hub, and this transition will be referred to as the hinging phase. Using similar methods as those described above, the hinge phase equations of motion are also determined. The
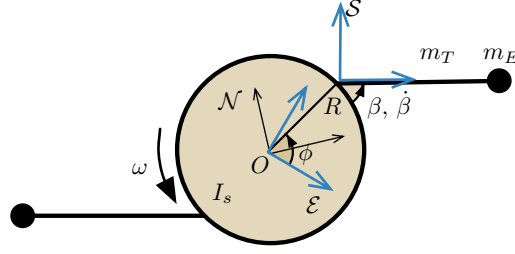
Figure 4: Hinging from tangential to radial dynamics parameters

parameters of interest are defined in Figure 4. The tether has freedom to rotate about the connection point by angle β, where the desired dynamics will come to rest at $\beta = 90 \deg$. The deployment angle ϕ is now fixed constant. The angular rate and velocities of the end mass and the tether center of mass are now described in the $\mathcal{S}$ frame.

$$\boldsymbol{\omega}_{\mathcal{S}/\mathcal{N}} = (\omega + \dot{\beta})\hat{\boldsymbol{s}}_3 \tag{15}$$

$$\dot{\boldsymbol{R}}_{E,H} = R\phi\hat{\boldsymbol{s}}_1 \tag{16}$$

$$\dot{\boldsymbol{R}}_{T,H} = -R\cos\beta\omega\hat{\boldsymbol{s}}_1 + \frac{1}{2}R((\phi + 2\sin\beta)\omega + \phi\dot{\beta})\hat{\boldsymbol{s}}_2 \tag{17}$$

The tether inertia for this phase is determined where the hinging position description is used. Only the third axis inertia is included in the planar dynamics.

$$I_{T,H_{33}} = \frac{1}{3}R^3\rho\phi(3 + \phi^2 + 3\phi\sin\beta) \tag{18}$$

These expressions define the kinetic energy state of the system expressed in Eq. 5c, and the Lagrange equations can now be used to determine the equations of motion for the hinging phase.

$$\frac{1}{2}R^2\phi\cos\beta(-2(m_E + R\rho\phi)\omega^2 + R\rho\phi\dot{\beta}^2) + \frac{1}{12}R^2\phi(12m_E\phi + R\rho(12 + 7\phi^2) + 6(2m_E + 3R\rho\phi)\sin\beta)\dot{\omega}+$$
$$\frac{1}{12}R^2\phi(12m_E\phi + R\rho(12 + 7\phi^2) + 12R\rho\phi\sin\beta)\ddot{\beta} = 0 \quad (19)$$

$$\frac{1}{12}R^2(24\phi(m_E + R\rho\phi)\cos\beta\omega\dot{\beta} + 6\phi(2m_E + 3R\rho\phi)\cos\beta\dot{\beta}^2)+$$
$$\frac{1}{12}R^2(6m_H + 12m_{T,0} + 12m_E(1 + \phi^2) + R\rho\phi(12 + 7\phi^2) + 24\rho(m_E + R\rho\phi)\sin\beta)\dot{\omega}+$$
$$\frac{1}{12}R^2\phi(12m_E\phi + R\rho(12 + 7\phi^2) + 6(2m_E + 3R\rho\phi)\sin\beta)\ddot{\beta} = u_s \quad (20)$$

B. Constant Spacecraft Rate in Tangential Deployment

A constant spacecraft rate is the simplest to implement and will be analyzed in detail here to provide a baseline case. The constant rate case is further valuable in that it provides insights into the deployment parameter relationships and behaviors. Additionally, it may be desirable in that it provides a predetermined reference trajectory and enables prediction of system behavior. Alternative objectives, such as tracking to maintain a constant tether tension, require live self observations and live updates of the reference trajectory, however in subsequent sections it is shown that these time varying cases will improve deployment time significantly. Looking at the tether tension expression:

$$\boldsymbol{T} = m_{E_i}R(\phi(\omega + \dot{\phi})^2 - \dot{\omega})\hat{\boldsymbol{s}}_R + m_{E_i}R(\omega^2 - \dot{\phi}^2 - \phi(\dot{\omega} + \ddot{\phi}))\hat{\boldsymbol{s}}_\phi \tag{21}$$

Where there is no tension in the $\hat{\boldsymbol{s}}_\phi$ direction, this portion of the expression can be set equal to zero. For a constant spacecraft rate, assuming the tether deployment is not accelerating, this expression can be used to prove that the deployment rate with respect to the spacecraft will be equal to the spacecraft spin rate

$$\omega = \dot{\phi} \tag{22}$$

Further applying these assumptions to the tension expression, the tether tension at a given point in the deployment is determined for an individual tether, i, from:

$$T_f = 4m_{E_i}\omega^2 R\phi \tag{23}$$

Additionally, assuming perfect tracking and constant rates, the torque required through the deployment duration is derived from the equations of motion to be

$$u_s = \frac{1}{12}R^2(30R\rho + 48m_E\phi + 42R\rho\phi^2)\omega^2$$

It is notable that the tension and torque do not rely on the spacecraft mass. These relationships can then be used to explore the sensitivity of the system to E-sail parameter choices. Of particular interest is the effect of the payload mass size on the rate requirements and deployment time. Where the maximum allowable tension in the Hoytether is known to be 0.05 N, the maximum allowable spin rate can be determined

$$\omega_{\max} = \sqrt{\frac{T_{\max}}{4m_{E_i}R\phi_f}} \tag{24}$$

Maps of these expressions as a function of the tether length, which can be determined from the deployment angle, and the payload end mass are displayed in Figure 5. These plots quickly demonstrate that for the constant spacecraft rate case, where the tension increases linearly over time and the maximum tension will be reached at the end of the deployment, the deployment reaches unreasonably long deployment times for large end mass payloads. One primary advantage of the E-sail propulsion in comparison to others is the relatively fast outer planet trajectory cruise times, which are on the order of 6-10 years for outer solar system destinations. If the sail requires nearly a year to deploy it will greatly impact the spacecraft acceleration and trajectory. Where the acceleration is most effective closer to the Sun, the E-sail deployment will most likely occur during the most propulsion-effective period of the trajectory (the exception being a case where the deployment is executed as the spacecraft ballistically approaches an inner planet flyby). This strongly motivates searching for time minimal deployment schemes that will reduce the impact on the E-sail effectiveness. Additionally, for smaller payloads, the torque required to reach the desired tension is well outside the range of feasible torque capabilities for modern spacecraft. This strongly motivates investigation of non-linear reference rate trajectories that will minimize deployment time while not exceeding torque capabilities.

C. Hub Rate Tracking Feedback Control Analysis

Lyapunov stability theory provides an analytical method to evaluate and develop controlled nonlinear dynamical systems using stability definitions and Lyapunov functions.[16] Using this method, a feedback control is developed that proves the hub-actuated, spacecraft-rate focused controller will be applicable and stable for this system. A positive definite Lyapunov function is chosen for this development and is defined in (25). It is desired that the spacecraft rate is controlled by a hub applied torque and tracks to a reference trajectory. Therefore, the Lyapunov function is only a function of the tracking error, $\delta\omega = \omega - \omega_r$.

$$V(\delta\omega) = \frac{\delta\omega^2}{2} \tag{25}$$

The time derivative of the Lyapunov function is now taken:

$$\dot{V}(\delta\omega) = \delta\omega\delta\dot{\omega} \tag{26}$$

To have asymptotic stability, the Lyapunov function must be negative definite. To find a control that guarantees this, (26) is set equal to a negative definite Lyapunov rate expression.

$$\dot{V}(\delta\omega) = -P\delta\omega^2 = \delta\omega\delta\dot{\omega} \tag{27}$$

Simplifying yields:

$$-P\delta\omega = \delta\dot{\omega} = \dot{\omega} - \dot{\omega}_r \tag{28}$$

where P is a positive gain. To determine the control torque, the expression for $\dot{\omega}$ as a function of torque, u_s, is substituted into Eq. (20) and u_s is solved for, shown in (29)

$$u_s = \frac{1}{24}R^2(-3(4R\rho + 8m_E\phi + 7R\rho\phi^2)\omega^2 + 3(5R\rho + 8m_E\phi + 7R\rho\phi^2)\dot{\phi}) +$$

$$+ \frac{1}{12}R^2\phi(15R\rho + 12m_E\phi + 7R\rho\phi^2)\ddot{\phi} - P\frac{1}{12}R^2\phi(18R\rho + 12m_E\phi + 7R\rho\phi^2)\delta\omega \tag{29}$$

a) max allowable body rate (deg/s)

b) required torque (N.m)
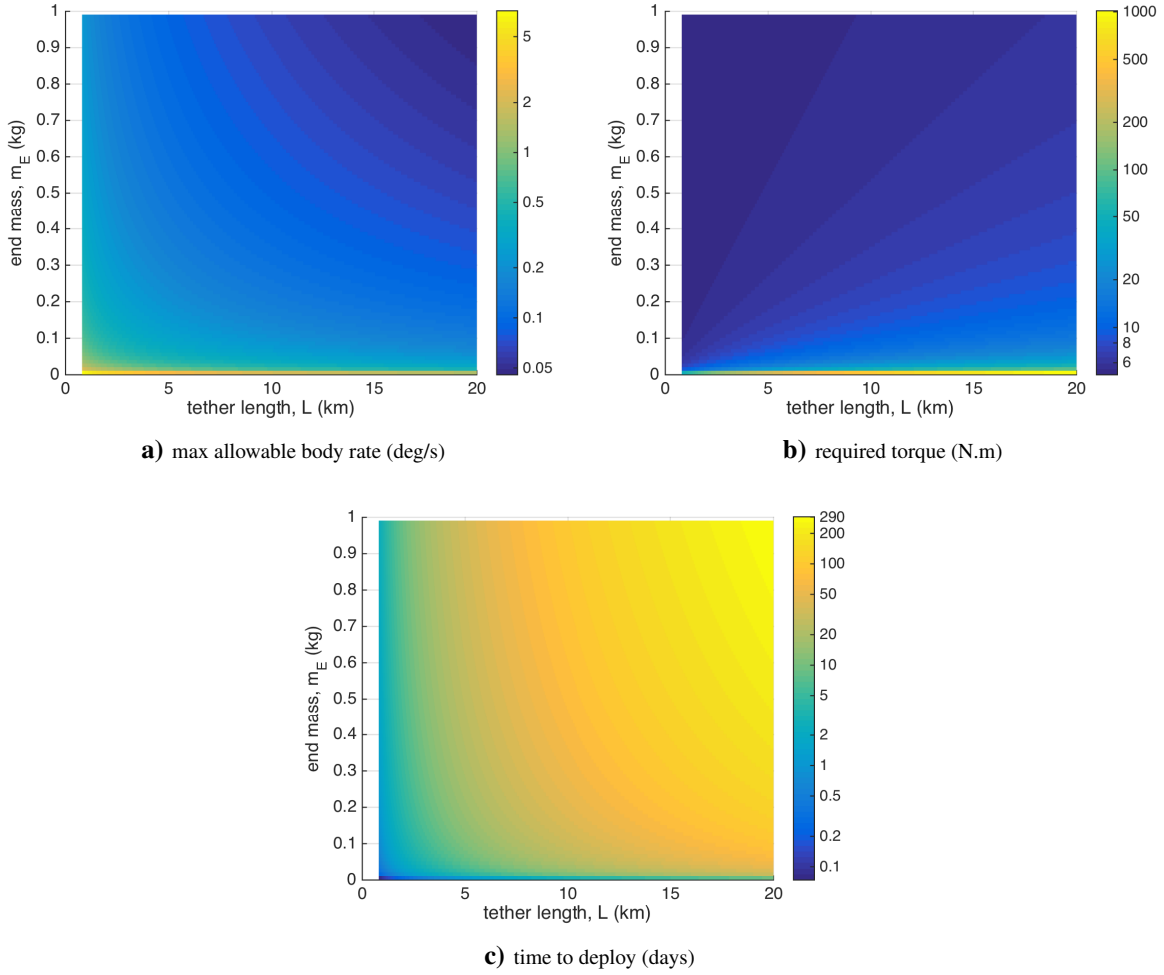

c) time to deploy (days)

Figure 5: Color maps of the maximum allowable spacecraft body rate and the corresponding torque required to maintain that rate and the time to deploy for the constant body rate case.

D. Spacecraft Rate Trajectory for Tension Maintenance

Alternatively, the spacecraft rate trajectory can be derived such that the tension is maintained constant. This allows for a time-minimum deployment, where the strength of material is treated as the limiting factor. To determine this reference rate, the time derivative of the tension expression is set equal to zero:

$$\dot{T} = mR(\dot{\phi}(\omega + \dot{\phi})^2 + 2\phi(\omega + \dot{\phi})(\dot{\omega} + \ddot{\phi}) + \ddot{\omega} = 0$$

Assuming there is no jerk, $\ddot{\omega} = 0$ and the relationship between the spacecraft rate and the deployment rate is determined as

$$\dot{\phi} = 2\omega$$

and the spacecraft rate required to provide constant tension as a function of deployment angle is

$$\omega^2 = \frac{T}{mR(9\phi - \frac{1}{\phi})}$$

The expression above cannot be used alone as a reference, where the expression is not defined for $\phi = 0$ and would exceed allowable rates for small ϕ. Therefore, a maximum allowable rate must be identified for the spacecraft and applied for the initial trajectory as a part of a piecewise approach, defined in Eq. (30). For simulation purposes, the maximum allowable spacecraft spin rate is set to 2.5 deg/s. The behavior for a deployment case where this is used as the reference speed is now compared to the constant rate case. Figure 6 shows the behavior over time for these two

cases, where the E-sail size parameters are chosen such that the characteristic acceleration is 0.1 mm/s² and there are 20 tethers, determining the tether length to be 4.3 km. The payload mass is set to a modest 50 grams to represent a low-mass actuator such as a photonic blade or independent sensor device.

$$\omega = \begin{cases} \omega_{\text{const}} & \omega_{\text{non-lin}} \geq \omega_{\text{max}} \\ \omega_{\text{non-lin}} & \omega_{\text{non-lin}} \leq \omega_{\text{max}} \end{cases} \qquad (30)$$

Table 1: Spacecraft and E-sail parameters implemented in example simulations.

$a_\oplus$ mm/s²	N	L m	m_{E_i} kg	m_T kg	m_H kg
0.1	20	4.3	0.050	0.996	500

E.   Numerical Simulations

a) body and tether rates

b) angular momentum of each component

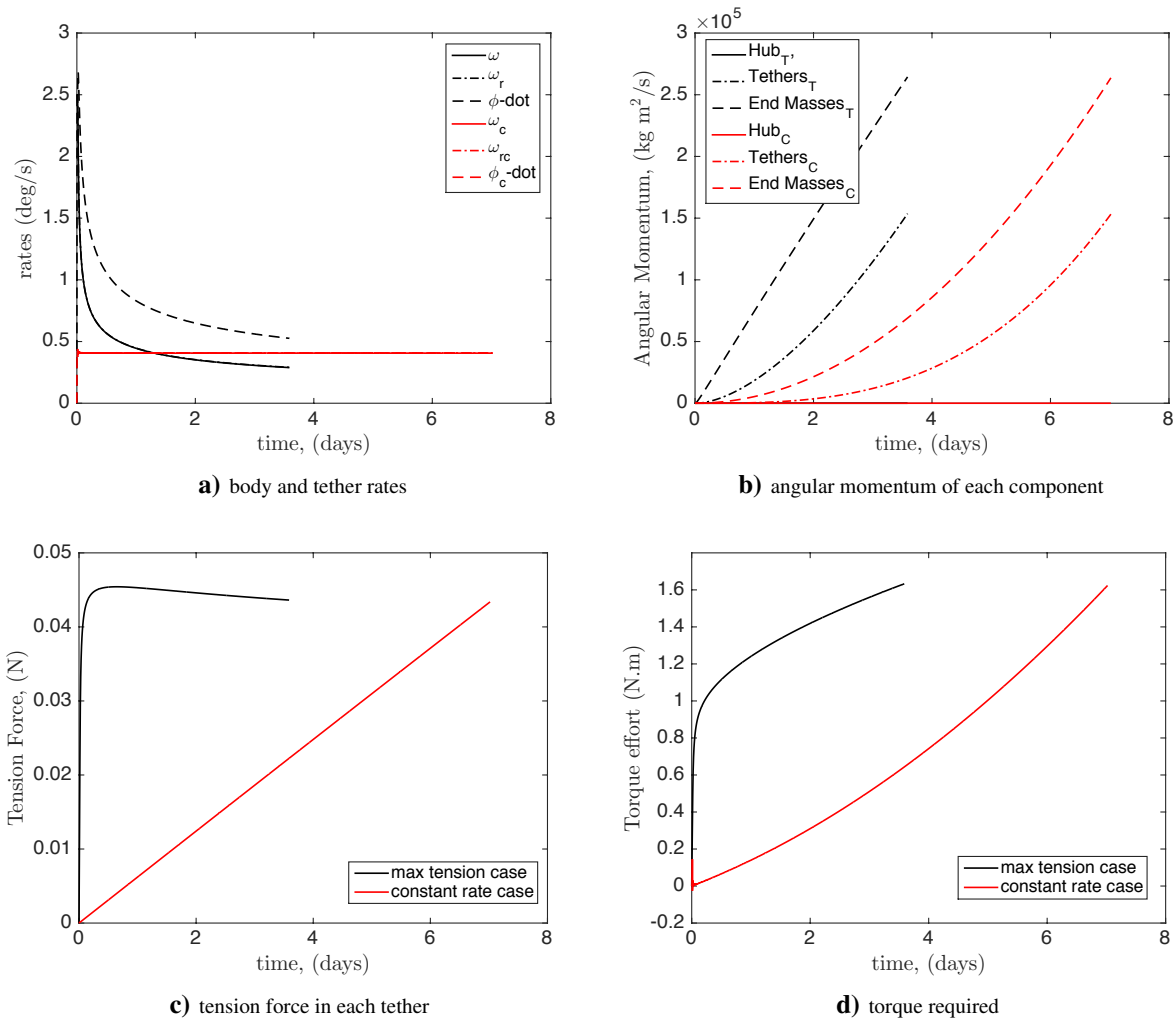**c)** tension force in each tether

d) torque required

Figure 6: Unwrap phase deployment of the tangentially deployed E-sail with a constant reference trajectory (black) and a tension derived trajectory (red).

The tension optimized reference trajectory is shown to decrease the deployment time from 7.02 days to 3.59 days, or to 51% of the constant rate deployment time. This is somewhat consistent with the expressions of expected deployment rate, Eq. (22) and Eq. (D.), which predict the tension derived reference will deploy at twice the hub rate.

a) body and tether rates

b) angular momentum of each component

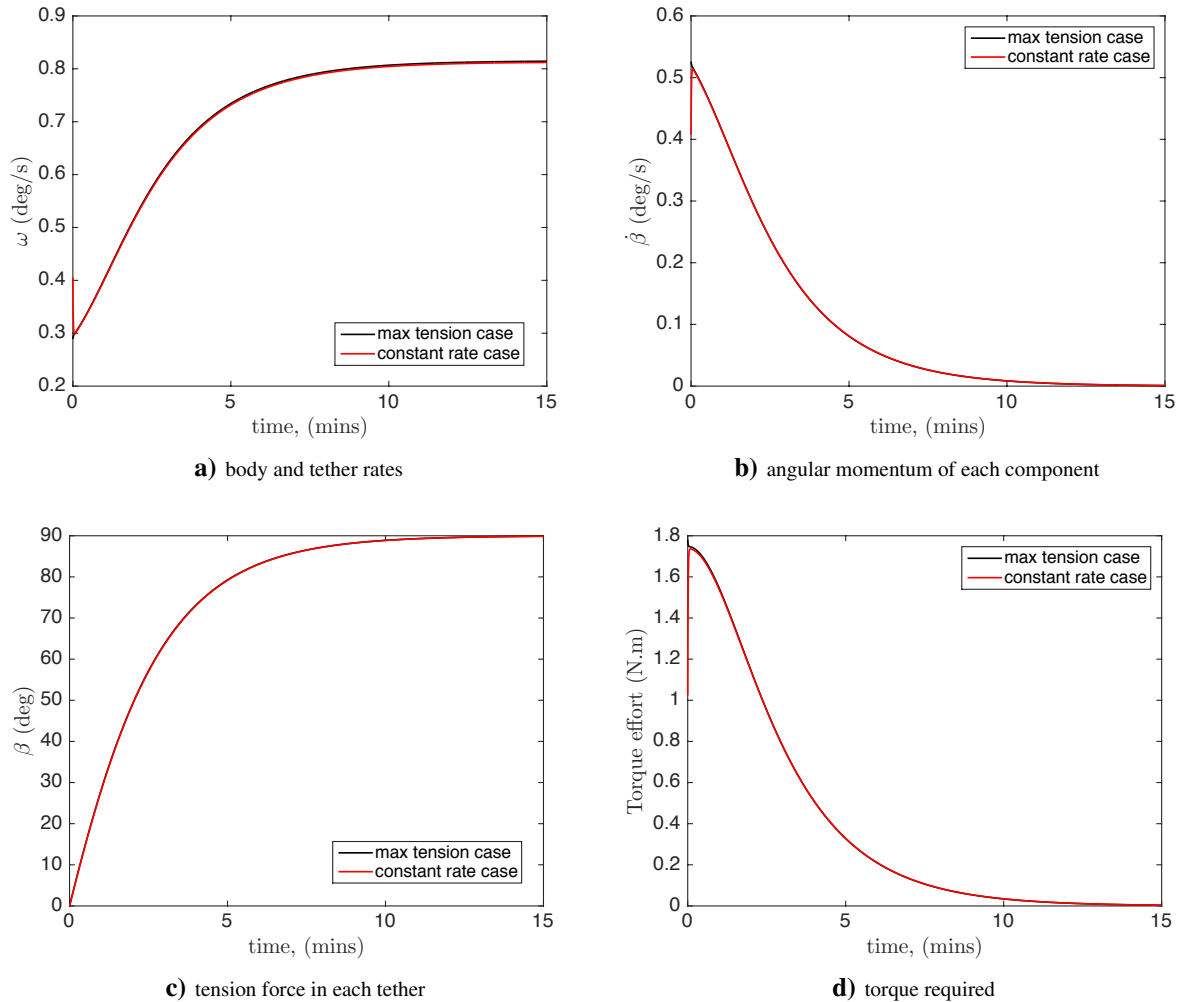**c)** tension force in each tether

d) torque required

Figure 7: The hinge phase of the tangentially deployed E-sail is shown to be the same for a constant reference trajectory (black) and a tension derived trajectory (red).

This is a significant savings and will be instrumental for deployment design, where the greatest strength of this concept is it's potential for implementing fast missions to the outer solar system and any time lost during deployment may detract from that. The tensions achieved at the end of the deployment are within 0.5% of each other, providing nearly equivalent end-tension cases. It is notable that the maximum torque capability needed to achieve the deployment is the same for both cases, however the maximum tension case has a higher average torque over the shorter duration. The hinge phase of both deployments are shown in Figure 7, and it's noted that the two cases have nearly identical hinging behaviors. Although there is a difference in the spacecraft rates at the start of deployment, at the moment hinging begins, the tether deployment rates, $\dot{\phi}$, are transfered to tether hinging rates, and the net behavior is the same. The applied torque ramps down as the tethers decelerate and transfer to the desired position and the hinging is completed smoothly in under 15 minutes. This shows that controlled hinging can be accomplished using the hub-mounted control scheme.

IV.   Radial Modeling and Parameter Analysis

Another method to deploy the E-sail is to use radially deploying tethers, as seen in Figure 8. Such a design requires tether reeling modules to stow and control each of the 20-100 tethers individually, and therefore requires 20-100 drive mechanisms. This introduces a large power consumption during the deployment as well as synchronization challenges. Additionally, the system still experiences significant momentum exchange and rate changes that couples with the unreeling process. However, this method enables highly valuable independent control of the tethers and
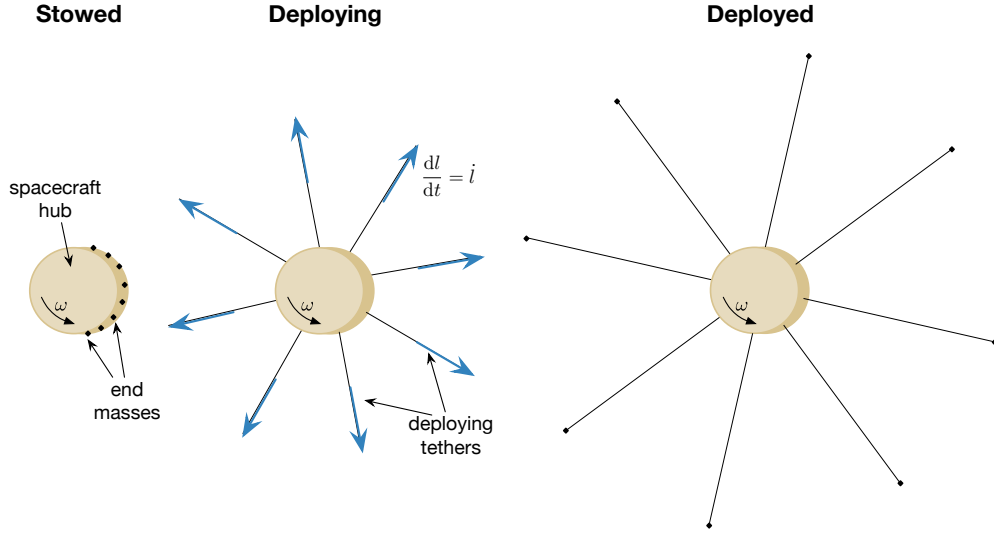
Figure 8: Various stages of the radial deployment scheme

decouples deployment failure risks of the tethers from each other. Furthermore, substantial engineering development has been done on a reeling mechanism.[12] Energy methods are used to determine the equations of motion for the radial deployment case.

A. Radial Deployment Equations of Motion

A dynamics model of this concept is developed using the simplified schematic illustrated in Figure 9. Here β is the angle of deviation of the tether from radial, and $\dot{\beta}$ is the rotation rate of the tether. The tether rotation with respect to inertial is

$$\boldsymbol{\omega}_{S/\mathcal{N}} = (\omega + \dot{\beta})\hat{\boldsymbol{s}}_3 \tag{31}$$

Then the velocity vectors are described in the $\mathcal{S}$ frame as

$$\dot{\boldsymbol{R}}_{E,H} = (\dot{l} + R\sin\beta\omega)\hat{\boldsymbol{s}}_1 + (l(\dot{\beta}+\omega) + R\cos\beta\omega)\hat{\boldsymbol{s}}_2 \tag{32}$$

$$\dot{\boldsymbol{R}}_{T,H} = \left(\frac{1}{2}\dot{l} + R\sin\beta\omega\right)\hat{\boldsymbol{s}}_1 + \left(\frac{1}{2}l(\dot{\beta}+\omega) + R\cos\beta\omega\right)\hat{\boldsymbol{s}}_2 \tag{33}$$

The radial tether inertia of the third axis is determined to be:

$$I_{T,H_{33}} = \frac{1}{12}\rho l^3 + \rho l((R\cos\beta + \frac{1}{2}l)^2 + R^2\sin\beta^2) \tag{34}$$
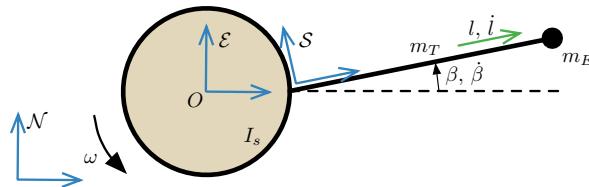

Figure 9: Radial deployment dynamics parameters

Using these definitions for the model components, the energy of the system is determined using Eq. (4). Using again the Lagrangian dynamics formulation, the coupled equations of motion for the hub rate ω and deflection angle

β are

$$\frac{1}{12}(6R\rho\sin\beta\dot{l}^2 - 12Rl\sin\beta m_E\dot{\beta}(\dot{\beta}+2\omega) - 6R\rho l^2\sin\beta\dot{\beta}(3\dot{\beta}+4\omega))+$$

$$\frac{1}{12}(3\dot{l}((4R^2\rho+7\rho l^2+8lm_E)(\dot{\beta}+\omega)+2R\cos\beta(4m_E(\dot{\beta}+\omega)+\rho l(7\dot{\beta}+8\omega))))+$$

$$\frac{1}{12}(12R^2\rho l+24R\rho\cos\beta l^2+7\rho l^3+24R\cos\beta lm_E+12l^2m_E+6R^2(2m_E+m_H+2m_{T,0}))\dot{\omega}+$$

$$\frac{1}{12}(12R^2\rho l+18R\rho\cos\beta l^2+7\rho l^3+12R\cos\beta lm_E+12l^2m_E)\ddot{\beta}=u_s \quad (35)$$

$$\frac{1}{12}(6Rl\sin\beta(-\rho l\dot{\beta}^2+2(\rho l+m_E)\omega^2))+$$

$$\frac{1}{12}(3\dot{l}((4R^2\rho+7\rho l^2+8lm_E)(\dot{\beta}+\omega)+2R\rho\cos\beta l(4\dot{\beta}+5\omega)))+$$

$$\frac{1}{12}(6R\cos\beta l(3\rho l+2m_E)+l(12R^2\rho+7\rho l^2+12lm_E))\dot{\omega}+$$

$$\frac{1}{12}(12R\rho\cos\beta l^2+l(12R^2\rho+7\rho l^2+12lm_E))\ddot{\beta}=0 \quad (36)$$

B. Radial Deployment with Constant Spacecraft Rate Case

Similarly to the tangential model analysis, the constant hub rate case can be further analyzed for the radial model. However unlike the tangential case, the deployment rate of the radial case is controlled by $\dot{l}$ which is assumed to be controlled by the spool motor and held constant. Therefore, adjustments in the reference rate will not result in a time savings. While including the deployment rate as a free variable is possible, it adds significant complexity to the model and is left for future work. For a radial orientation, the tether tension is written as

$$\boldsymbol{T} = m(R\cos\beta\omega^2+l(\dot{\beta}+\omega)^2)\hat{\boldsymbol{s}}_R - m(R\sin\beta\omega^2+2\dot{l}(\dot{\beta}+\omega)+l\ddot{\beta}))\hat{\boldsymbol{s}}_\phi \quad (37)$$

where there is no tension in $\hat{\boldsymbol{s}}_\phi$, the tether normal direction, the following are known:

$$T = m_{E_i}(R\cos\beta\omega^2+l(\dot{\beta}+\omega)^2) \quad (38)$$

$$-m(R\sin\beta\omega^2+2\dot{l}(\dot{\beta}+\omega)+l\ddot{\beta})) = 0 \quad (39)$$

Assuming the tether's position is not changing or accelerating, $\dot{\beta}=0$ and $\ddot{\beta}=0$, Equation 39 is used to solve for an expression of β:

$$\beta = \sin^{-1}\frac{-2\dot{l}}{R\omega} \quad (40)$$

This result proves that for a radially deploying spin stabilized tether, there must be some deviation from the radial orientation during deployment. This is a significant result that implies a trade between the deployment rate, spacecraft rate, and tether position deviation. Due to the assumptions made in the derivation, there is some deviation from the predicted position and the observed position in numerical simulations. However, the prediction is within 2% accuracy. Furthermore, by this definition, the quantity including the ratio of the linear deployment rate to the spacecraft rate must be from 0-1 for the tether position to be defined. This limits the possible rate configuration of the system.

C. Lyapunov Control Stability Analysis

Similarly to the tangential case, the Lyapunov function for the radial deployment is only a function of the tracking error, $\delta\omega = \omega - \omega_r$, and the same Lyapunov function and derivation methods are applied here. To determine the control torque, the expression for $\dot{\omega}$ as a function of torque, u_s, is substituted into Eq. (35) and u_s is solved for. This

derivation assumes a constant reference rate.

$$u_s = \frac{1}{12}(6R\rho \sin \beta \dot{l}^2 - 12Rl \sin \beta m_E \dot{\beta}(\dot{\beta} + 2\omega) - 6R\rho l^2 \sin \beta \dot{\beta}(3\dot{\beta} + 4\omega)) +$$
$$\frac{1}{12}(3\dot{l}((4R^2\rho + 7\rho l^2 + 8lm_E)(\dot{\beta} + \omega) + 2R\cos \beta(4m_E(\dot{\beta} + \omega) + \rho l(7\dot{\beta} + 8\omega)))) +$$
$$\frac{1}{12}(12R^2\rho l + 18R\rho \cos \beta l^2 + 7\rho l^3 + 12R\cos \beta lm_E + 12l^2 m_E)\ddot{\beta}$$
$$- P\frac{1}{12}(12R^2\rho l + 24R\rho \cos \beta l^2 + 7\rho l^3 + 24R\cos \beta lm_E + 12l^2 m_E + 6R^2(2m_E + m_H + 2m_{T,0}))\delta\omega \quad (41)$$

Spacecraft Rate Trajectory for Tension Maintenance

Considering instead the time-minimum approach where the tension force in the tether is maximized and maintained constant, assuming the tether's position is not changing or accelerating, and that there is no jerk on the spacecraft hub, the position of the tether can be predicted as

$$\beta = \sin^{-1}\frac{-3\dot{l}}{2R\omega} \quad (42)$$

Which is similar to what is determined for the constant rate case, where there is a factor of 2 in the constant expression and a factor of 3/2 here, indicating that this reference trajectory maintains a smaller tension deviation than the constant case. The spin rate trajectory corresponding with this is determined as a function of the current tether deployment length and rate as

$$\omega = \sqrt{\frac{8T(2\rho L + m_{E_i}) + \rho m_{E_i}\dot{l}^2}{m_{E_i}(4R^2\rho + 23\rho l^2 + 16lm_{E_i})}} \quad (43)$$

D.   Numerical Simulation

The response of the system to this reference trajectory is illustrated in Figure 10 along with the the constant rate case. The deployment rate, $\dot{l}$, in both cases is equivalent and constant, however, so the time to deploy is equivalent. However, the tether angle in the time varying trajectory is notably smaller, and the magnitude of the torque effort required is smaller, despite maintaining a higher tension. This analysis does not account for the additional spin up phase prior to deployment. The discontinuity in the position angle occurs at the switch of the piecewise reference trajectory, and is attributed to the derived expressions of the tether position angle for the two cases. Eq. (42) and Eq. (40) show that the predicted tether position will change, and the numerical simulation reflects this discontinuity. As in the tangential case, due to the tether position displacement, a hinging maneuver will need to be executed at the end of the deployment. Figure 11 illustrates the hinging for these two cases. The constant rate case, which has more displacement from radial, is shown to require a slightly more time and a greater torque effort to complete the transition, but overall these two cases show similar behavior.

V.   Conclusions and Future Work

The two E-sail deployment schemes investigated in this paper provide feasible means to actuate the deployment of an E-sail structure using hub mounted torque only. The tangential deployment scheme provides a simpler deployment for lower torque, however it removes the ability to control the individual tether spooling. Deployment in a truly radial configuration, where $\beta \approx 0$, is shown to require much greater spin rates or much longer deployment duration than allowing tethers to drift. The advantage of an ideal radial deployment is that a hinge phase would not be needed, however in practical application it is shown that allowing hinging will greatly reduce the deployment time or hub spin rate requirements. The radial deployment configuration was developed based on the individual tether spooling concept. Modifying the individual spools to orient the deployment to a tangential configuration would be worth considering in future simulations, and may provide the optimal deployment.

The deployment torque can be applied to the hub using a variety of methods, depending on the order of magnitude and duration of torque needed for the deployment. Electric thrusters are ideal candidates for their range of thrust magnitudes and time varying capabilities for smaller inertia E-sails. Reaction wheels could also be used if fine control is needed, however the momentum stored in the wheels would need to be actively removed. Chemical thrusters may also be used to achieve large torques for large E-sails, however the time variations could only be achieved using pulse width modulation thrust. The effects of such an approach on the deployment dynamics must be investigated to ensure stability. Incorporating realistic thruster models to the deployment simulation is left to future work.
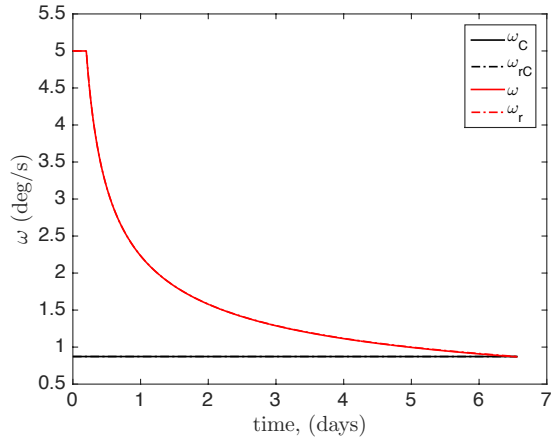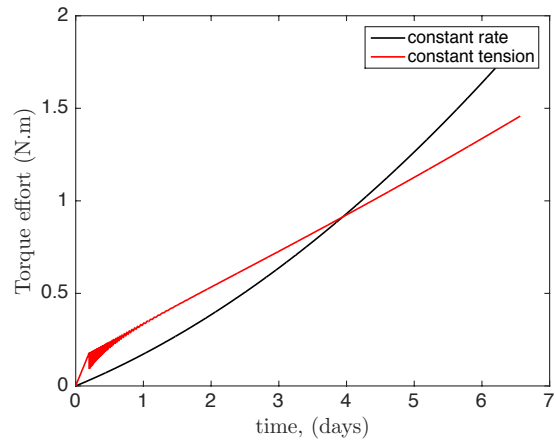
a) body and tether rates
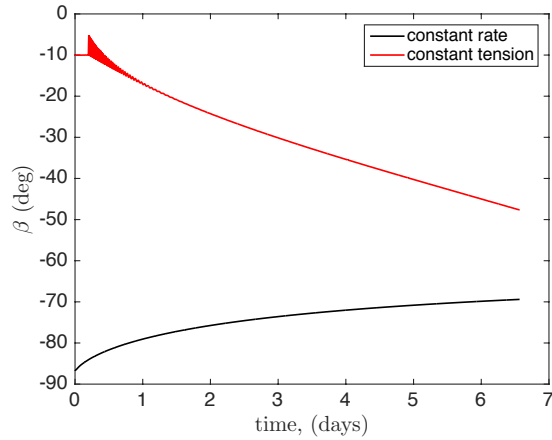
b) angular momentum of each component
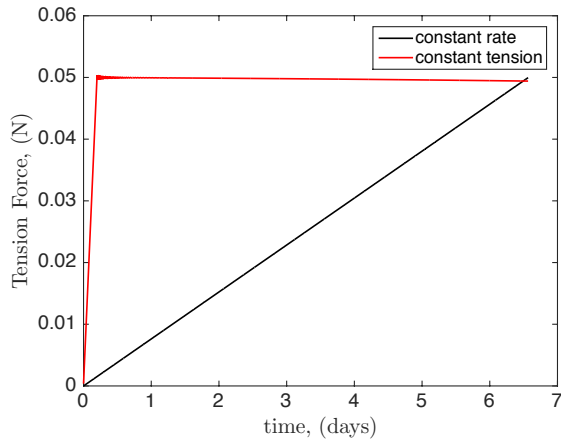
c) tension force in each tether

d) torque required

Figure 10: Behaviors of the radially deployed E-sail with a constant reference trajectory (black) and a tension derived trajectory (red).

The spacecraft rate trajectory, deployment rate, characteristic acceleration, and tether tip mass are large contributors to the deployment dynamics and must be chosen judiciously. Defining realistic boundaries for these parameters based on technology capabilities and mission requirements will inform future simulations. Additionally, it is determined that E-sails designed to have a greater number of shorter tethers have smaller inertia and therefore require less energy and momentum to deploy. However, these tethers would be in closer proximity to each other and may present collision risks. State error estimation of the tether positions must be done to determine the closest allowable proximity of two adjacent tethers. Future work will model each tether individually with a unique state and determine the factors influencing variation in position to do this. Permitting tether hinging raises concern that the flexible tethers may exhibit in-plane bending despite internal tension. Model fidelity will therefore be further increased by using a lumped-mass method to incorporate the flexibility of the tethers. While many questions on the finer behavior of the E-sail deployment remain, the baseline momentum and torque requirements of the hub actuated deployment are now defined.

a) body and tether rates

b) angular momentum of each component

c) tension force in each tether
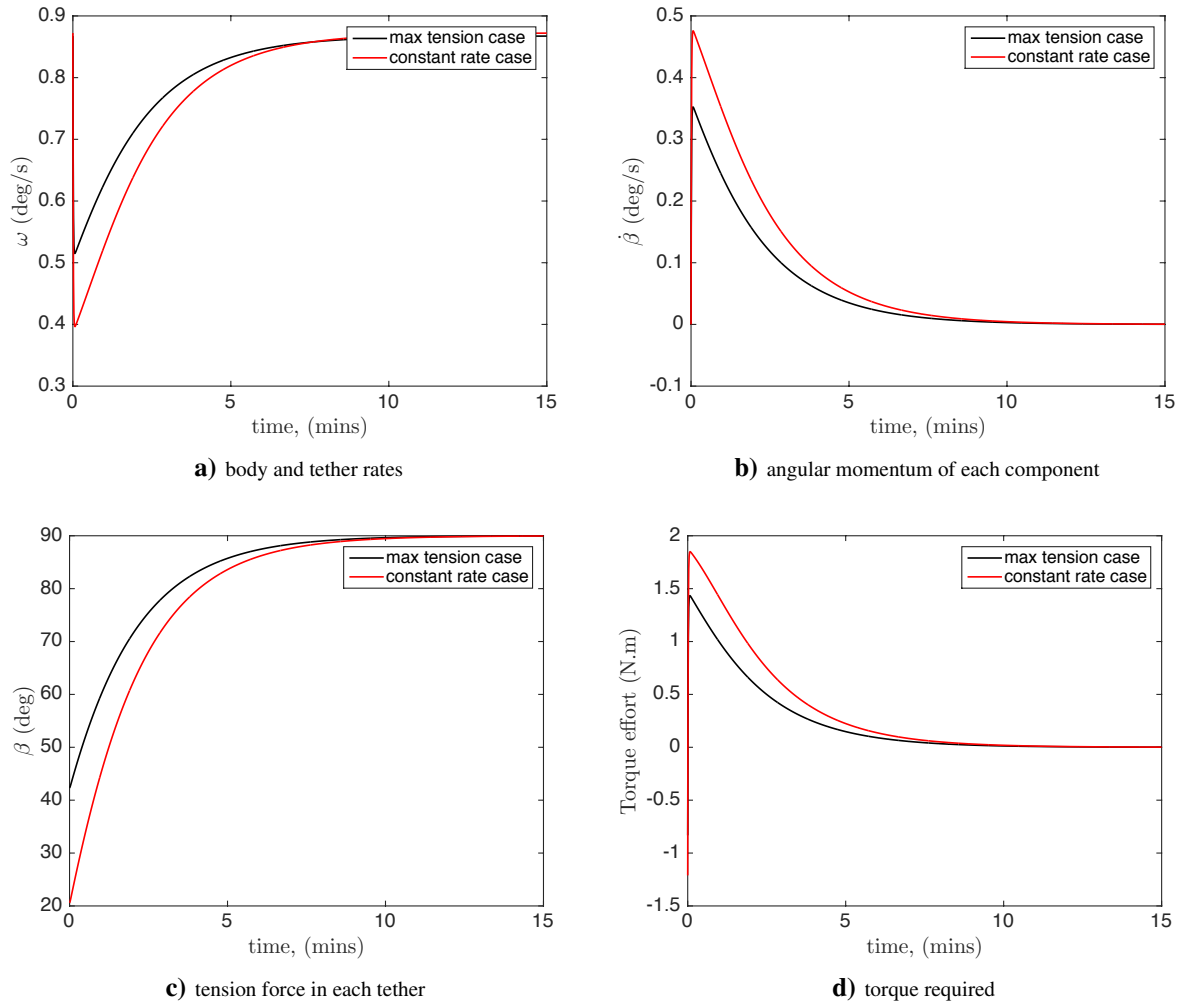

d) torque required

Figure 11: The hinging phases of the radially deployed E-sail deployment with a constant reference trajectory (black) and a tension derived trajectory (red) are slightly different due to the difference in initial tether angle.

References

[1] Janhunen, P., "Electric Sail for Spacecraft Propulsion," *Journal of Propulsion and Power*, Vol. 20, No. 4, 2004.

[2] Janhunen, P., "The electric sail - a new propulsion method which may enable fast missions to the outer solar system," *Journal of the British Interplanetary Society*, Vol. 61, No. 8, 2008, pp. 326–329.

[3] Janhunen, P. and Sandroos, A., "Simulation study of solar wind push on a charged wire: basis of solar wind electric sail propulsion," *Annales Geophysicae*, Vol. 25, 2007, pp. 755–767.

[4] Les Johnson, R. M. Y. and IV, E. E. M., "Status of Solar Sail Propulsion: Moving Toward an Interstellar Probe," *AIP Conference Proceedings*, Vol. 886, 2007, pp. 207–214.

[5] Szames, A.

[6] Pekka Janhunen, J. Lebreton, S. M., "Fast E-sail Uranus entry probe mission," *Planetary and Space Science*, Vol. 104, 2014, pp. 141–146.

[7] Wiegmann, B., "Heliopause Electrostatic Rapid Transit System (HERTS)," June 2014.

[8] Quarta, A. A. and Mengali, G., "Electric Sail missions to potentially hazardous asteroids," *Acta Astronautica*, Vol. 66, 2010, pp. 1506–1619.

[9] Mengali, G. and Quarta, A. A., "Electric Sail Performance Analysis," *Journal of Spacecraft and Rockets*, Vol. 45, No. 1, 2008, pp. 122–129.

[10] Hoyt, R. and Forward, R. L., "Alternate interconnection Hoytether failure resistant multiline tether," 2001.

[11] Timo Rauhala, Henri Seppänen, J. U. S. K. G. M. P. J. and Hæggström, E., "Automatic 4-wire Heytether production for the Electric Solar Wind Sail," *International Microelectronics Assembly and Packing Society Topical Workshop and Tabletop Exhibition on Wire Bonding*, 2013.

[12] R. Rosta, O. Kromer, T. Z. P. J. K. T. Z. P. J., "Wrecker: an unreeling mechanism for a thin electrically conductive space tether," *CEAS Space Journal*, Vol. 7, 2015, pp. 53–68.

[13] et al., A. S., "ESTCube-1 in-orbit experience and lessons learned," *Aerospace and Electronic Systems Magazine, IEEE*, Vol. 30, 2015, pp. 12–22.

[14]Janhunen, P., "Recent Advances in Electric Sail Development," *Numerical Modeling of Space Plasma Flows: Astronum-2008*, Vol. 406, 2009, pp. 135–140.

[15]P. Janhunen, A. Quarta, G. M., "Electric solar wind sail mass budget model," *Geoscientific Instrumentation, Methods and Data Systems*, Vol. 2, 2013, pp. 85–95.

[16]Schaub, H. and Junkins, J. L., *Analytical Mechanics of Space Systems*, American Institute of Aeronautics and Astronautics, Inc., 1801 Alexander Bell Drive, Reston, Virginia, 20191-4344, 3rd ed., 2014.